Sterically Encumbered 4,5-bis(diphenylphosphino)acenaphthene ligand and its Ni(II), Pd(II), Pt(II), and Cu(I) complexes.

Massimo Tosolini,[a] João Avó,[b] António Jorge Parola,[c] Gabriele Balducci,[a,*] and Paolo Tecilla[d,*]

a) Dr. M. Tosolini, Dr. G. Balducci
Department of Chemical and Pharmaceutical Science, University of Trieste, Via Giorgieri 1, 34127 Trieste, Italy. E-mail: balducci@units.it
http://www.dscf.units.it/ricerca_grp.php?name=inorgani1group&menu=group&file=balducci
b) Dr. J. Avó
IBB-Institute for Bioengineering and Biosciences, Instituto Superior Técnico, Universidade de Lisboa, Lisbon, Portugal.
c) Prof. A. J. Parola
LAQV–REQUIMTE, Department of Chemistry, NOVA School of Science and Technology, Universidade NOVA de Lisboa, Campus da Caparica, 2829-516, Caparica, Portugal.
d) Prof. P. Tecilla
Department of Mathematic and Geosciences, University of Trieste, Via Weiss 2 1, I-34127 Trieste, Italy. E-mail: ptecilla@units.it
https://www.units.it/persone/index.php/from/abook/persona/5958

Abstract: A new sterically encumbered symmetrically substituted 4,5-bis(diphenylphosphino)acenaphthene ligand (**L**) has been prepared. The ligand readily forms distorted square planar complexes with group 10 metal ions (Ni(II), Pd(II), Pt(II)) and a dimeric tetrahedral complex with Cu(I). The X-ray structure of the ligand and of the complexes show a notably short distance between the two phosphorus atoms, well below than twice the van der Waals radius of P, due to the steric requirements of the rigid acenaphthene backbone. Moreover, in the complexes a stabilizing π-π interaction between two phenyl rings belonging to the two P atoms is present. The **$[LCuCl]_2$** complex is weakly fluorescent both in solution and in the solid state with higher quantum yield as a solid where it exhibits thermally-activated delayed fluorescence and phosphorescence. **$[LPdCl_2]$** and **$[LCuCl]_2$** behave as chloride transporters across a liposomal phospholipid membrane with the Pd(II) complex displaying a very high activity.

Introduction

The development of chelating diphosphine ligands has been a prolific research area since 1959 when the first diphosphine ligand, 1,2-bis(diphenylphosphino)ethane (dppe), has been reported.[1] Since then a large number of bidentate phosphine ligands and their complexes with late transition metals have been prepared and characterized.[2, 3, 4] The interest in these ligands and complexes is largely motivated by their use in the homogeneous catalysis of several highly relevant reactions such as, for example, metal-catalyzed cross coupling reactions[5] and catalytic asymmetric hydrogenation.[6] More recently, metal complexes of diphosphine ligands have been exploited as purely structural building blocks for the self-assembling of complex supramolecular structures[7] in a controlled and predictable manner following the so-called metal-mediated directional-bonding approach.[8] For example, the square planar [Pd(dppp)$(OTf)_2$] complex has two labile coordination positions with coordination geometry of 90° and combination of this fragment with a linear ditopic ligand led to the formation of a self-assembled 4+4 square metallacycle (dppp: 1,3-bis(diphenylphosphino)propane).[9]

Following our interest in the development of artificial ionophores,[10] we became involved in the chemistry of diphosphine Pd(II) complexes when trying to assemble tubular supramolecular structures in liposomes using as building blocks a functionalized *trans* 5,15-di-(4-pyridyl)-porphyrin and [Pd(dppp)$(OTf)_2$] with the aim to obtain a trans-membrane channel able to transport ions across the phospholipid membrane.[11,12] In the membrane environment the Pd(II) complex failed in driving the self-assembling process but we discovered that the [Pd(dppp)$(OTf)_2$] itself as well as the dichlorido analogue, [Pd(dppp)(Cl_2)], behave as efficient ionophores exchanging anions across the membrane with a carrier type mechanism.[13] Moving from this observation we started a systematic search among different diphosphine ligands in order to analyze the ligand effect on the ionophoric activity of the complex.[14]

Among the structurally different diphosphine ligands we were attracted by those deriving from the rigid acenaphthene core bearing two functionalized P(III) donors in the *peri*-position (Figure 1).[15, 16] In this ligand, as well as in the structurally related 1,8-bis(diphenylphosphino)naphthalene (dppn, Figure 1),[17] the rigid structure of the aromatic backbone forces the two phosphorus atoms in the *peri*-position at a distance well below the sum of their van der Waals radii. These free ligands are characterized by a bite angle of ca. 90°, close to that of dppp but locked in a more rigid planar structure.[18] The chemistry of the acenaphthene di-substituted in *peri*-position with large atoms and groups has been disclosed by Petr Kilian and co-workers who prepared and studied several acenaphthene derivatives symmetrically and unsymmetrically substituted with phosphorus, tin,

thallium, antimony, bismuth , etc.[19, 20, 21,22, 23] Furthermore, a systematic study on acenaphthene derivatives *peri*-substituted with a diphenylphosphino group and elements of groups 13 and 15 has been reported by Chęcińska, Beckmann, and coworkers.[24] Recently, the group of Kilian has reported a detailed study of the coordination chemistry of the unsymmetrical ligand *i*Pr_2P-Ace-PPh_2 (Figure 1) with several transition metal ions showing that the ligand forms square planar complexes with group 10 d^8 metal ions ([(*i*Pr_2P-Ace-PPh_2)MX_2], M = Ni, Pd, Pt; X = Cl, Br).[15, 25] This type of complexes are potentially relevant for our studies on anion carriers but we realized that the simple symmetric Ph_2P-Ace-PPh_2 (**L**, Figure 1) was not described in the literature. We therefore prepared Ph_2P-Ace-PPh_2 and here we describe its synthesis and the characterization of the ligand and of its complexes with Pd(II), Pt(II), Ni(II), and Cu(I), including single-crystal X-ray structure determination, along with a preliminary study of the ionophoric activity of the Pd and Cu complexes.

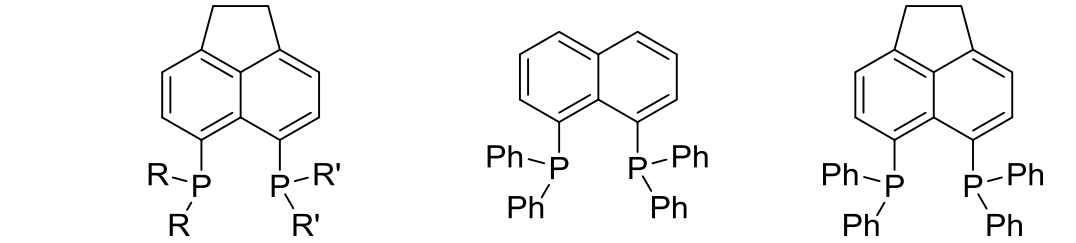

iPr_2P-Ace-PPh_2 : R = Ph, R' = *i*Pr dppn Ph_2P-Ace-PPh_2 (**L**)

Figure 1. Structure of ligands *i*Pr_2P-Ace-PPh_2, dppn, and Ph_2P-Ace-PPh_2 (**L**).

Results and Discussion

Synthesis of ligand Ph_2P-Ace-PPh_2 and of its metal complexes

Peri-substituted bis-phosphino acenaphthenes are usually prepared from 5,6-dibromoacenaphthene by stepwise halogen-lithium exchange followed by P−C coupling with the desired chlorophosphine.[25] In this scheme the two phosphorus substituents are introduced on the aromatic scaffold in two different steps preparing first the 5-bromo-6-phosphino derivatives and, after a second bromine-lithium exchange, the bis-phosphine compound thus allowing to obtain also non-symmetrically substituted acenaphthenes. However, being our target a symmetrically substituted derivative we attempted a single step reaction in which the bis-lithium derivative was produced directly from 5,6-dibromoacenaphthene using 2 equivalents of *n*-BuLi and reacted with

chlorodiphenylphosphine. Using the standard condition and in particular THF as solvent the reaction provided a mixture of mono and bis-substituted acenaphthene derivatives, even when a large excess of Ph_2PCl was used. Moreover, since the mono and bis-substituted products have almost the same R_f on silica, they are very difficult to separate. However, changing the solvent to Et_2O and increasing the concentration of the starting material caused the precipitation of the bis-substituted product driving the reaction to completion. Once the synthesis was optimized (Scheme 1), the ligand L could be obtained on a multigram scale, up to 5 grams, with good yield (90%) and without the need of purification by chromatography. Ligand **L** is stable in the solid state for weeks while it slowly oxidizes to the corresponding phosphine oxide in solution. On the other hand, the bis-phospino oxide can easily be obtained by reaction of **L** with H_2O_2 in DCM.

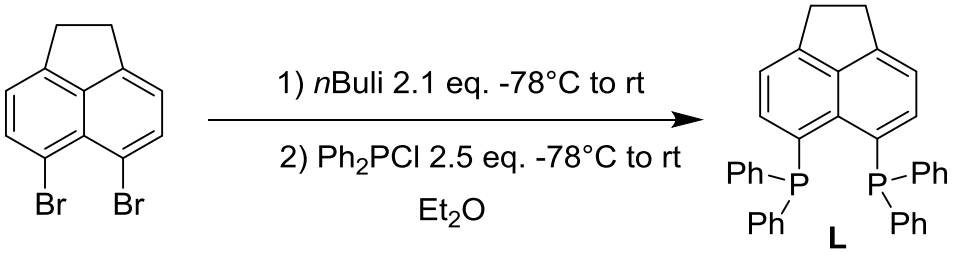

Scheme 1. Synthesis of ligand Ph_2P-Ace-PPh_2 (**L**).

The synthesis of the metal complexes of ligand **L** prepared in this work is reported in Scheme 2. All the complexes were characterized by ESI-MS, elemental analysis, IR, UV-Vis and Fluorescence spectroscopies and, where possible, by ^1H, ^{13}C and ^{31}P-NMR. Reaction of **L** with $(MeCN)_2PdCl_2$, $Pt(cod)Cl_2$ or $NiCl_2$ in methanol led to the precipitation of complexes **[LPdCl$_2$]**, **[LPtCl$_2$]** and **[LNiCl$_2$]** in 61%, 70% and 85% yield, respectively. All the three complexes are mononuclear with the metal ion adopting an approximate square planar geometry. While the Pd and Pt complexes are colorless the Ni(II) one is red colored. The copper complex was obtained in 55% yield adding directly CuCl to a chloroform solution of **L** and subsequent precipitation of the complex as gold powder by addition of Et_2O. In the solid state the complex is dinuclear with two chlorides bridging the two Cu(I) ions which assume a tetrahedral geometry. However, as reported for Cu(I) complexes with chelating *bis*-phosphine ligands,[26] it is likely that in solution **[LCuCl]$_2$** dissociates forming species of different stoichiometry as signaled by the broad peaks in the ^1H and ^{31}P NMR spectra recorded in CD_2Cl_2. The NMR signals remain broad in CD_3CN and became slightly sharper in DMSO-D_6, suggesting that the solvent may influence the dissociation equilibrium (Figures S6 and S7). In any case the 1:1 stoichiometry of the complex was confirmed by elemental analysis and

ICP-MS while ESI-MS showed the presence of both $[LCu]^+$ and $[(LCu)_2Cl]^+$ fragments, suggesting that in solution the complex might exist in both the mononuclear and dinuclear form (Figure S8).

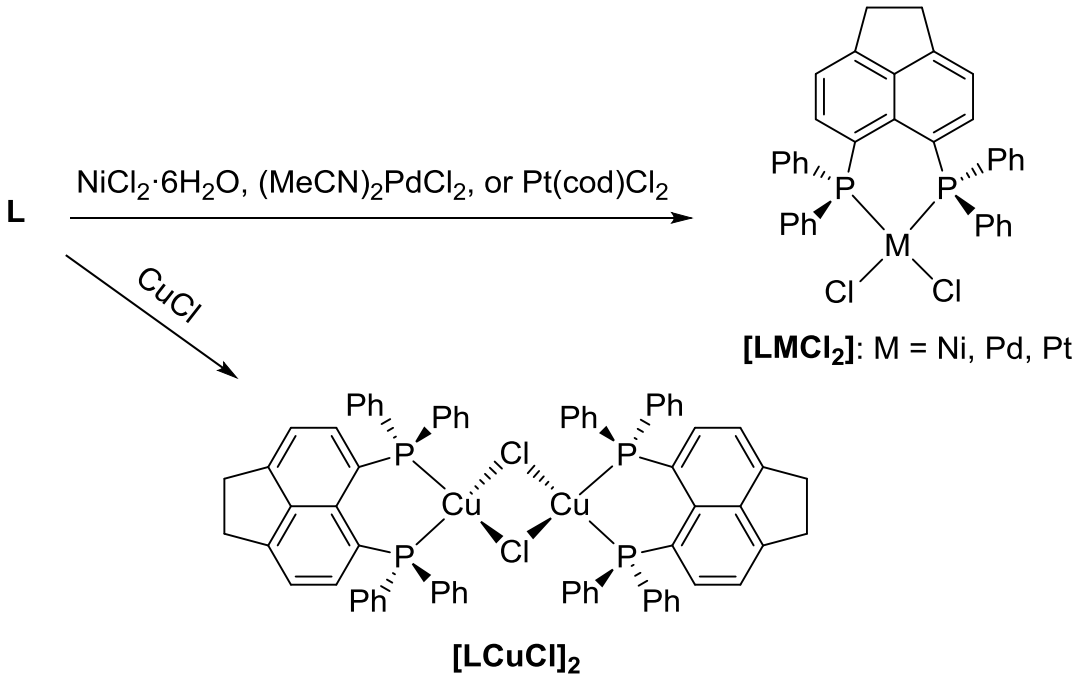

Scheme 2. Synthesis of metal complexes of ligand Ph_2P-Ace-PPh_2 (**L**). cod = *cis*, *cis*-1,5-cyclooctadiene.

Single crystal X-ray diffraction analysis

Crystals of **L** suitable for X-ray crystallography were obtained by slow evaporation from a CD_2Cl_2 solution. The compound crystallized in the monoclinic centrosymmetric space group P 2_1/n. The molecular structure of **L** is shown in Figure 2. Relevant interatomic bond lengths and angles are listed in Table1 while further crystallographic information is reported in the Supporting Information.

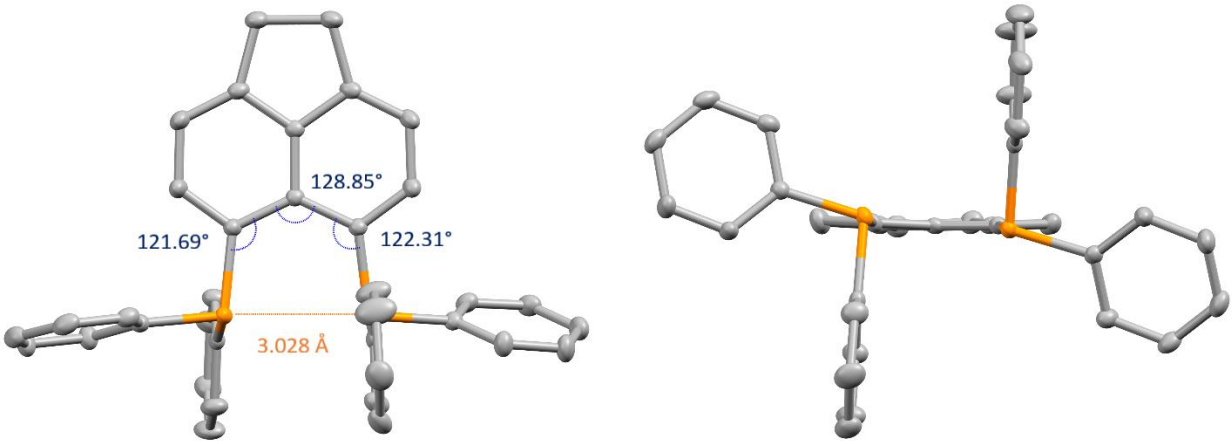

Figure 2. Ball and stick molecular representation of ligand **L** showing the top and side view of the molecular structure. The bond angles (deg) of the bay area are reported in blue, the distance between P1 and P2 is reported in orange (Å). (C gray, P orange, hydrogen atoms are omitted for clarity).

In the molecular structure of **L** the rigid structure of the acenaphthene backbone forces the two P atoms at a distance of 3.028 Å which is 16% shorter with respect to that expected from the van der Waals radius of P (1.8 Å)[27]. The repulsion that arises from the proximity of the two atoms results in a distortion of the bond angles in the bay area. The splay angle, defined as the sum of the angles of the bonds in the bay area minus 360°, describes the distortion in substituted naphthalenes and acenaphthenes. In the case of **L** the splay angle is 12.85°, similar to its naphthalene analogue, 1,8-bis(diphenylphosphino)naphthalene (12.78°)[28], but much larger with respect to the unsubstituted acenaphthene (7.88°).[29] Further indicators of the structure distortion are the out-of-plane displacement of the phosphorus with respect to the mean plane of the acenaphthene backbone atoms (-0.124 and 0.109 Å for P1 and P2, respectively) and the P2-$C_{ipso(acenaphthene)}$--$C_{ipso(acenaphthene)}$-P1 torsion angle. Overall, the crystal structure of **L** is very similar to that reported for the analogue unsymmetrical ligand *i*Pr_2P-Ace-PPh_2 with a slightly shorter P···P distance and slightly smaller splay angle (3.100(2) Å and 14.3° in *i*Pr_2P-Ace-PPh_2, respectively).[15]

Table 1. Selected interatomic distances [Å] and angles [deg] for **L** and its metal complexes.

compound	**L**	**[LNiCl$_2$]**	**[LPdCl$_2$]**	**[LPtCl$_2$]**	**[LCuCl]$_2$**
P1···P2	3.0280(6)	3.0702(7)	3.1449(8)	3.112(1)	3.2492(6)
P1–M		2.1590(5)	2.2384(4)	2.2273(8)	2.2291(4)
P2–M		2.1720(8)	2.2430(5)	2.2213(8)	2.2372(4)
splay angle[a]	12.8	15.2	17.2	15.0	17.9
P1–M–P2		90.29(2)	89.14(2)	88.77(3)	93.35(2)
out-of-plane displacement[b]					
P1	-0.124	0.154	0.179	-0.315	0.407
P2	0.109	0.017	0.294	0.277	-0.157
M		0.913	1.306	0.907	1.278
metal complex fragment[c]		28.68	37.50	35.53	43.20
peri-region torsion angle					
P2- $C_{ipso(acenaphthene)}$ ––$C_{ipso(acenaphthene)}$-P1	6.23(6)	5.11(7)	2.67(8)	15.5(2)	13.99(8)
π-π stacking					
Distance of the centroids of the two phenyls		3.890	3.689	3.797	3.671
C_{ipso}–P1––P2–C_{ipso} torsion angle		6.62(6)	1.62(7)	18.9(5)	15.73(7)
Angle between the two phenyl planes		14.37	8.05	7.40	4.17

a) the sum of the bay region angles -360° (see Figure 2); b) displacement from the acenaphthene mean plane; c) Angle between the acenaphthene mean plane and the mean plane of the metal complex fragment.

Crystals of the metal complexes of **L** suitable for X-ray crystallography were obtained by slow diffusion of ethyl ether in a solution of the metal complex in $CHCl_3$. The crystal structures of the four complexes are shown in Figure 3 and selected crystallographic data are reported in Table 1. In the case of **[LNiCl$_2$]** two molecules of very similar geometry are present in the asymmetric unit. In all cases **L** behaves as bidentate ligand with the two P atoms involved in metal coordination forming a six member chelate ring.

The metal atoms in the complexes of Ni(II), Pd(II) and Pt(II) adopted a distorted square planar geometry with the P1–M distance marginally shorter than the P2–M one in the complexes with Ni(II) and Pd(II) and with the two phosphorus atoms slightly displaced from the Cl1–M–Cl2 plane, the highest deviation being observed in **[LNiCl$_2$]** in which one P atom lies 0.434 Å above the plane. The effect of the metal ion coordination on the bay region is small with an increase in the P1⋯P2 distance and of the splay angle. The largest effect is observed in the Pd(II) complex with an increase of 0.1169 Å and 4.4° of the P1⋯P2 distance and splay angle, respectively, in comparison to the free ligand. Also the displacement of the two P atoms from the acenaphthene is marginally increased. This is reflected in a twisting of the acenaphthene plane with respect to the mean plane of the metal fragment (M–Cl1–Cl2–P1–P2) of 28.68°, 37.50° and 35.35° for the Ni(II), Pd(II), and Pt(II) complexes, respectively. In all the three metal complexes one phenyl substituent of the P points outward (Ph1 in Figure 3) while the other (Ph2 in Figure 3) faces the phenyl ring on the other phosphorous atom (Ph3 in Figure 3) in an almost parallel orientation engaging stabilizing π-π interactions.[30] The angle between the plane of the two facing phenyl rings varies from 7.40° in the Pt(II) complex to 14.37° in **[LNiCl$_2$]** and the distance between the two centroids of the aromatic rings is within 3.689 (Pd(II)) and 3.890 (Ni(II)) Å. The mutual orientation of these phenyl rings in the three complexes is slightly different: while in **[LPdCl$_2$]** the two phenyls form an almost perfect sandwich type dimer they are increasingly laterally displaced and partially rotated on going from Ni(II) to Pt(II) complex. This is reflected by the torsion angle C_{ipso}–P1−−P2–C_{ipso} that increases from 1.62° to 18.9° on going from the Pd(II) to the Pt(II) complex. These differences are most probably due to the crystal packing. In the case of the Pt and Ni complexes the acenaphthene group of one molecule experiences the close interaction of a Ph group of another molecule (Pt complex) or a solvent $CHCl_3$ molecule (Ni complex): the greater torsion angle measured for these complexes is thus the result of the distortion induced by these "close contacts" in the acenaphthene moiety; on the other hand, in the case of the Pd complex no close intermolecular interactions are present around the acenaphthene, thus allowing for a higher planarity of the whole P1-acenaphthene-P2 molecular region.

In the solid state the Cu(I) complex is dinuclear with two chlorides bridging the two Cu(I) ions. In this centrosymmetric dimer the metal ions adopt a tetrahedral geometry with the P2–Cu2 distance marginally longer than the P1–Cu1 distance. In comparison with the structure of the free ligand, in **[LCuCl]$_2$** the strongest increase in the P1⋯P2 distance is observed (+ 0.22 Å) together with a moderate increase of the splay angle (+ 5.1°), of the *peri*-region torsion angle (+ 7.76°) and of the displacement of the P atoms from the mean acenaphthene plane. This leads to an angle between the acenaphthene and P1–Cu1–P2 planes of 43.2°. Also in this complex two phenyls, each belonging to

a different phosphorous atom, face each other engaging π-π stacking interactions. The two phenyls are almost parallel with an angle between the two phenyl planes of only 4.17°, a distance between the two centroids of 3.671 Å, and a C_{ipso}–P1—P2–C_{ipso} dihedral angle of 15.73° reflecting a partial rotation and lateral displacement.

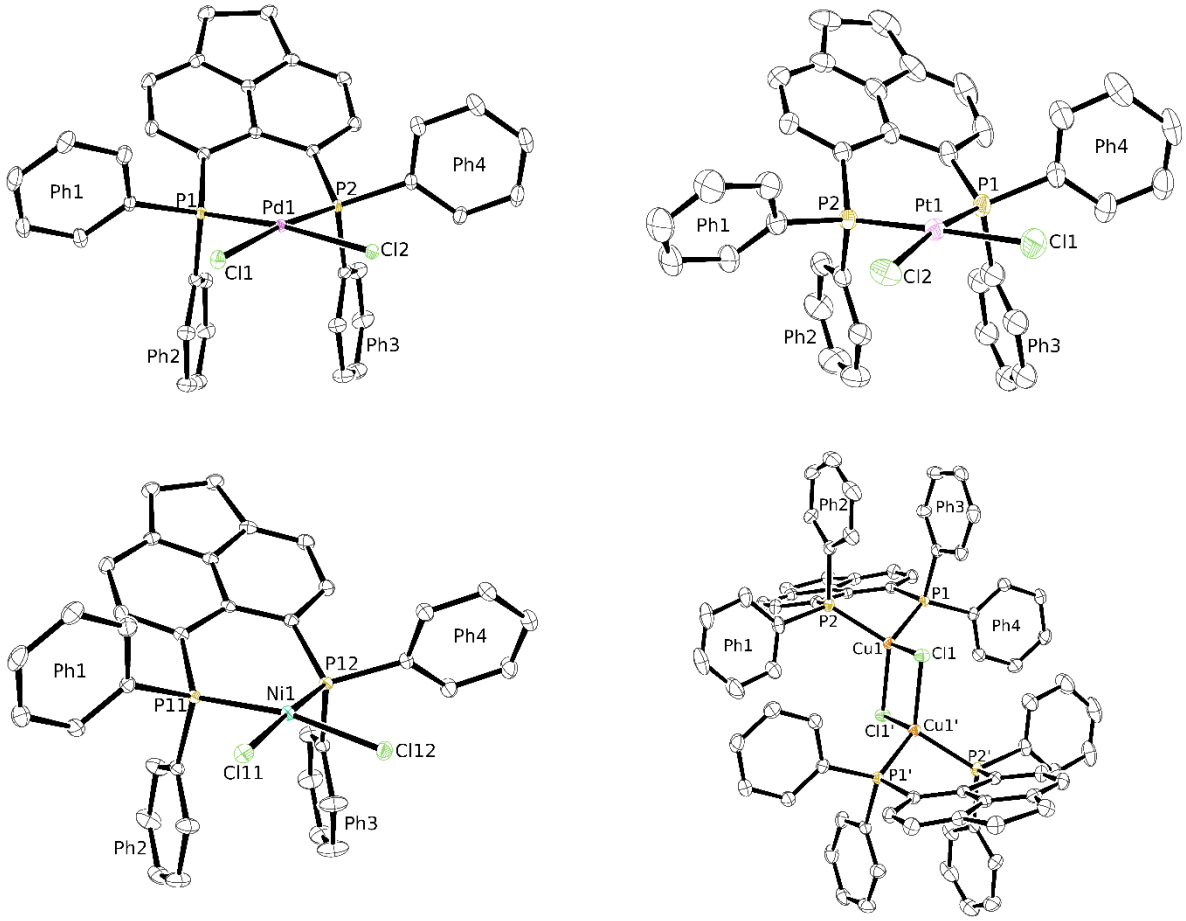

Figure 3: ORTEP representation (50% probability ellipsoids) of the molecule of complexes **[LPdCl$_2$]**, **[LPtCl$_2$]**, **[LNiCl$_2$]** and **[LCuCl]$_2$** in the crystal structure. Solvent molecules as well as hydrogen atoms have been omitted for clarity. For the same reason, only major populations of disordered groups are represented. For **[LNiCl$_2$]**, only one of the two crystallographically independent molecules is shown. For **[LCuCl]$_2$**, primed atom labels indicate symmetry mates.

*Photophysical Properties of ligand **L** and of their metal complexes*

The UV-Vis, emission and excitation spectra of ligand **L** recorded in DCM are shown in Figure 4. The UV-Vis spectrum is characterized by a strong absorption below 250 nm and a less intense band centered at 300 nm ($\varepsilon = 1.7 \cdot 10^4$ $M^{-1}cm^{-1}$) which can be reasonably assigned to a π-π* and n-π* transition, respectively. The ligand is weakly fluorescent with an emission band centered at 380 nm

upon excitation at 300 nm. The excitation spectrum recorded at 375 nm shows a band with a maximum at 325 nm, superimposed to the lower energy UV-Vis absorption.

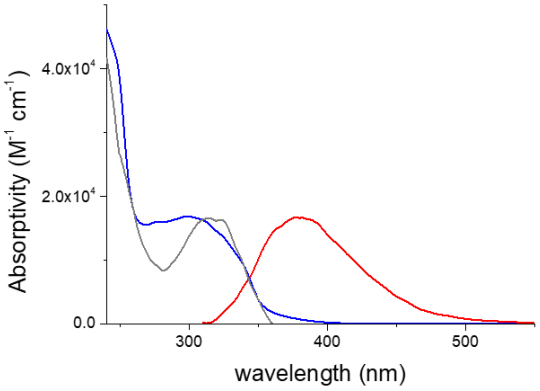

Figure 4: UV-Vis (blue), normalized fluorescence emission (red, λ_{exc} = 300 nm) and normalized excitation (grey, λ_{em} = 375 nm) spectra of **L** (4.50 x 10^{-5} M) in DCM.

The UV-Vis spectra of the metal complexes of **L** in DCM are reported in Figure 5. In the case of Pd(II) and Pt(II) the most relevant modification of the spectra with respect to that of the ligand alone is the disappearance of the band at 300 nm and the appearance of a new band of similar intensity and shifted to 355 and 330 nm, respectively, that can be attributed to a charge transfer transition (CT). The spectra of Ni(II) and Cu(I) complexes are more complex. In the case of **[LNiCl$_2$]** there is a very broad ligand-centered absorption (LCT) at 304 nm with a shoulder at 370 nm and a weak absorption band at 485 nm (ε = 508 $M^{-1}cm^{-1}$), while in the spectra of **[LCuCl]$_2$** the more symmetric LCT is centered at 310 nm and the charge transfer (CT) band at 400 nm (see also below).

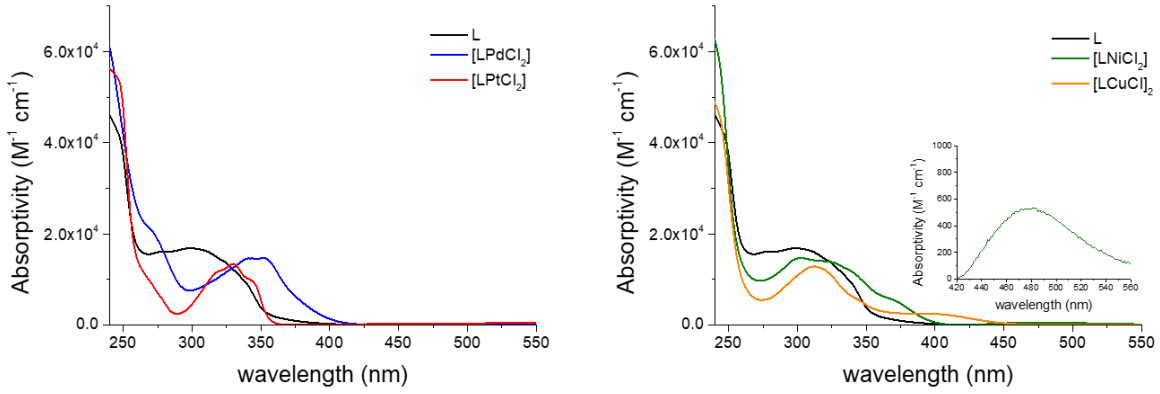

Figure 5: UV-Vis spectra of ligand **L** (black), **[LPdCl$_2$]** (blue), **[LPtCl$_2$]** (red), **[LNiCl$_2$]** (green), and **[LCuCl]$_2$** (gold), in DCM. Inset shows the weak absorption band of **[LNiCl$_2$]**.

Complexation with the metal ions resulted in an almost total quenching of the fluorescence emission of **L** (Figure S9) with the exception of the copper complex which shows orange emission when irradiated with the UV lamp (365 nm) in the solid state (Figure S10). Because fluorescent ionophores are potentially important for localization studies in living cells we investigated the photophysical properties of this complex in more detail.

Complex **[LCuCl]$_2$** exhibits significant solvatochromism with absorption and emission spectra varying with solvent polarity, although we cannot exclude some influence of the different solvents on the dissociation of the complex in solution (see above). In any case, in most solvents, **[LCuCl]$_2$** exhibits two absorption bands, one at ca. 310 nm that does not vary significantly with solvent polarity, corresponding to the ligand-centered absorption (LCT) and a band the maximum of which varies significantly with solvent polarity, that can be attributed to a charge transfer transition (CT).[31] Two bands are also detectable in emission spectra: the LCT is detectable at ca. 400 nm and the CT appears as a broad band with maxima from 550 nm to 620 nm, depending on solvent polarity (Figure 6 and Table 2).

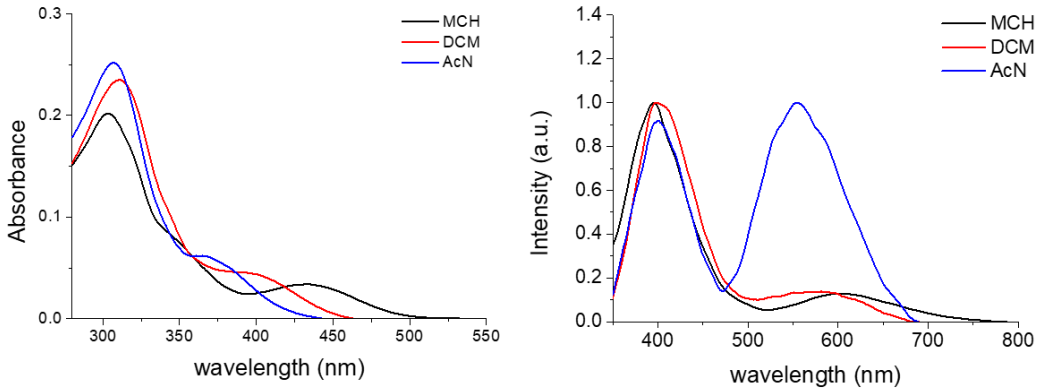

Figure 6: Absorption (left) and emission (right) spectra of compound **[LCuCl]$_2$** (10 mM) collected in methylcyclohexane (black), dichloromethane (red) and acetonitrile (blue). The spectra collected in the other solvent listed in Table 2 are reported in Figure S11.

Table 2: Absorption (λ_{abs}) and emission (λ_{em}) maxima (nm) of **[LCuCl]$_2$** determined in different organic solvents

solvent	λ_{abs} (LCT)	λ_{em} (LCT)	λ_{abs} (CT)	λ_{em} (CT)
Methylcyclohexane	304	395	432	603
Toluene	326	400	364*	n.d.
Dichloromethane	310	406	396	n.d.
Acetonitrile	307	401	368*	555
Dimethylsulfoxide	306	410	n.d.	541
Methanol	303	384	380*	569

* undefined band/shoulder

In the solid state, compound **[LCuCl]$_2$** exhibits a single emission band centered at 607 nm, which can be attributed to the CT transition (Figure 7). This photoluminescence is sensitive to oxygen, increasing ca. 1.5 times upon degassing. This increase in luminescence intensity is due to the contribution of a long-lived emission (τ = 387 μs), which is detectable with time-resolved emission spectroscopy. Luminescence maxima (λ_{em}), prompt (PF) and delayed (DF) fluorescence quantum yields (Φ) and lifetimes (τ) of **[LCuCl]$_2$** in solution (acetonitrile) and solid state (amorphous powder) are summarized in Table 3. These results suggest that part of **[LCuCl]$_2$** luminescence arises from triplet states, and since both steady state and time resolved emission show the same spectrum, it is proposed that **[LCuCl]$_2$** exhibits thermally-activated delayed fluorescence (TADF).[32] To corroborate this hypothesis, the luminescence intensity of the delayed emission was measured as a function of excitation energy and it was observed to be strictly linearly dependent (Figure 7c), evidencing the unimolecular origin for this emission.[33]

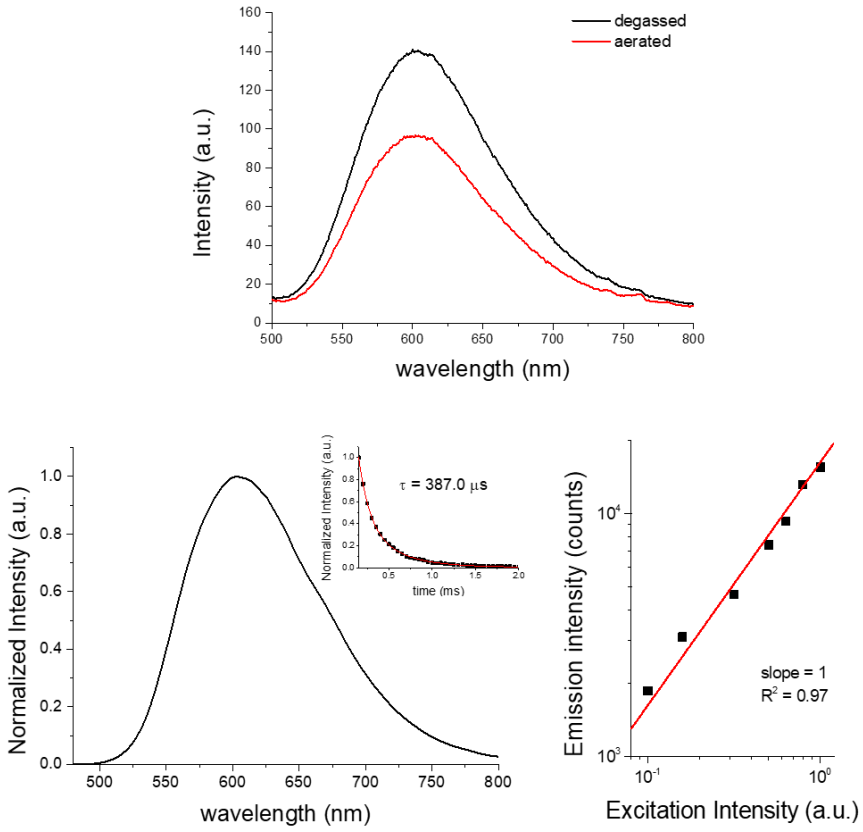

Figure 7: a) steady state emission spectra of **[LCuCl]$_2$** in solid state, collected at room temperature in vacuum (black) and in contact with air (red), λ_{ex} = 450 nm; b) time-resolved emission spectrum of **[LCuCl]$_2$** in solid state collected at room temperature, λ_{ex} = 450 nm, delay = 0.15 ms, integration time = 0.5 ms. Inset shows the intensity decay collected at 610 nm, fitted with a mono exponential function with τ = 0.39 ms; c) variation of time-resolved emission intensity as a function of excitation intensity. The linear fit with slope fixed at 1 demonstrates the unimolecular origin of this emission.

At 77 K, the solid-state emission changes significantly, appearing as a broad band centred at ca. 650 nm, which is attributed to the phosphorescence of **[LCuCl]$_2$**. From the emission spectra at room-temperature and 77 K, it is possible to estimate the S_1-T_1 energy gap (ΔE_{ST}) using the spectroscopic method (140 meV, from delayed fluorescence maximum = 607 nm; phosphorescence maximum = 652 nm).[33]

Using time-resolved spectroscopy, an additional long-lived luminescence was also observed, with a lifetime significantly longer than the phosphorescence of **[LCuCl]$_2$** (9.40 vs. 1.45 ms, respectively). This emission, centered at ca. 580 nm, can be attributed to the ligand-centered $T_1 \rightarrow S_0$ transition.

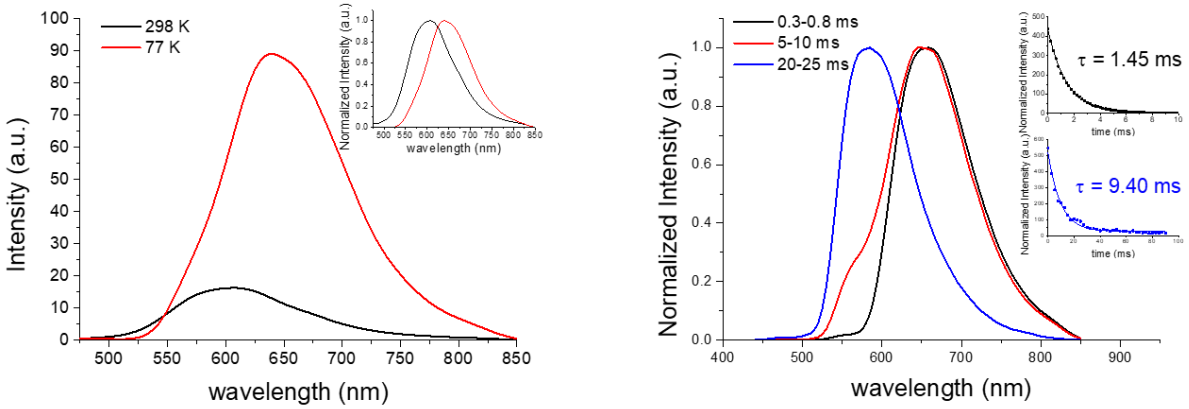

Figure 8: a) steady state emission spectra of compound **[LCuCl]$_2$** in solid state, collected at room temperature (black) and 77 K (red) in contact with air, λ_{ex} = 450 nm, the inset shows the normalized emission spectra; b) time-resolved emission spectrum of **[LCuCl]$_2$** in solid state collected at 77 K using different delay and integration times: from 0.30 to 0.80 ms (black), from 5.0 to 10.0 ms (red) and from 20 to 25 ms (blue), λ_{ex} = 450 nm. Inset shows the intensity decays collected at 580 nm (blue) and 680 nm (black), fitted with a mono exponential function with τ = 9.40 ms and τ = 1.45 ms, respectively.

Table 3: Photophysical parameters determined for **[LCuCl]$_2$** in solution (acetonitrile) and solid state (amorphous powder) at room temperature.

	λ_{em} (nm)	Φ_{PF}	τ_{PF} (ns)	Φ_{DF}	τ_{DF} (ms)
Solution	400/564	0.006	0.850	n.d.*	n.d.*
Solid State	602	0.015	0.360	0.007	0.387

* not detected

Ionophoric activity

As illustrated in the Introduction, diphosphine Pd(II) complexes and in particular **[dpppPdCl$_2$]** are able to transport chloride ions across a phospholipid membrane by an anion exchange mechanism.[13] We, therefore, tested the ionophoric activity of **[LPdCl$_2$],** to have a direct comparison with the previously studied complex, and of **[LCuCl]$_2$** because a fluorescent ionophore could be useful in biological studies where the localization of the compound in living cells has to be determined,[34] although the low luminescence quantum yield of the complex may represent a limit for practical application.

The ionophoric activity of the two complexes was investigated with the HPTS assay (Figure 9).[35] In this test HPTS (8-hydroxypyrene-1,3,6-trisulfonic acid), a fluorescent pH indicator with a pK_a of 7.2, is trapped in the inner water pool of large unilamellar vesicles (LUVs, 100 nm diameter) made by egg yolk phosphatidylcholine (EYPC). The lipid suspension is prepared in water buffered at pH 7 and containing 100 mM NaCl. Then a pH gradient is established across the phospholipid membrane by external addition of NaOH. The increase of the HPTS fluorescence emission in response to the applied transmembrane pH-gradient indicates basification of the inner water pool which may be derived either from H^+ efflux or OH^- influx. This transmembrane charge translocation needs to be counterbalanced by a concurrent movement of other ions and in the case of **[dpppPdCl$_2$]** it has been shown that the complex promoted a OH^-/Cl^- antiport in which the transport of OH^- from outside to inside the liposome is balanced by the opposite transport of a chloride ion (Figure 9).[13] Therefore, the increase in HPTS emission is directly related to the transport of chloride across the phospholipid membrane.

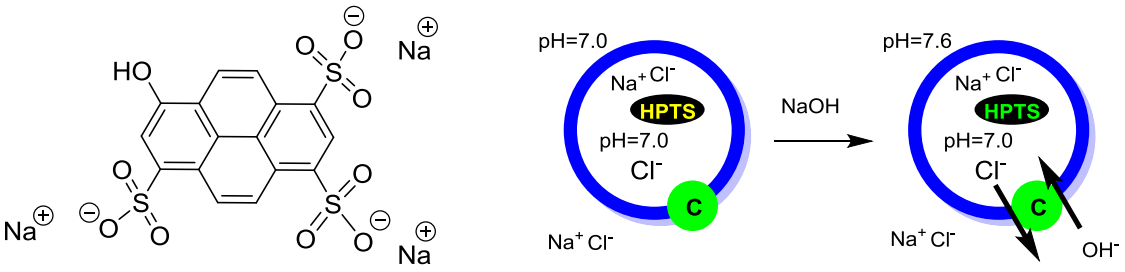

Figure 9: Structure of HPTS (left) and schematic illustration of the HPTS assay (right) in which a carrier (C, green circle) promotes the antiport of OH^- and Cl^-.

Figure 10 reports typical kinetic traces obtained with the HPTS assay. The kinetic is made in a fluorimetric cuvette containing the liposome suspension and the metal complex. After 50 seconds a

base pulse is applied by addition of NaOH starting the OH^-/Cl^- antiport process. This is signaled by an increase in the fluorescence emission which follows a first order kinetic law. After 350 seconds the vesicles are lysed by addition of a surfactant (Triton X-100) allowing to measure the maximal intensity of fluorescence which is then used to normalize the data (see the Experimental Section). Both metal complexes showed appreciable transport activity in comparison with the control experiment recorded in their absence (black trace). The **$[LPdCl_2]$** is the most active also taking in consideration that the kinetic reported in Figure 10a (blue trace) is recorded at a concentration of metal complex ten times lower with respect to the concentration of **$[LCuCl]_2$** used for recording the red kinetic profile (the concentration of ionophore in Figure 10 is given as % with respect to the total concentration of lipids). Similar experiments were repeated for different concentrations of metal complexes and the kinetic profiles were fitted with a first-order-rate equation to obtain the apparent rate constants for the transport process (k_t, s^{-1}, Figure 10b/c). The activity concentration profiles show an increase of activity on increasing the concentration of metal complex with an upward curvature which has been observed also in the case of **$[dpppPdCl_2]$** and that was interpreted in terms of participation to the transport process of dimeric metal species.[13] **$[LPdCl_2]$** is by far more active than **$[LCuCl]_2$** and, interestingly, it is also more active than the **$[dpppPdCl_2]$** complex. Indeed, at a 0.04 % concentration of metal complex the rate constants measured for **$[LPdCl_2]$** and **$[dpppPdCl_2]$** were 0.17 s^{-1} and 0.0075 s^{-1}, respectively, which corresponds to a 22-fold acceleration. This result together with the activity, although more modest, showed by the fluorescent copper complex is particularly interesting when taking into account that the lipophilicity of these complexes has not been optimized. Indeed, it has been shown that lipophilicity is one of the most important parameters influencing the activity of such type of carriers.[14] It is, therefore, reasonable to imagine that, a fine tuning of the lipophilicity of the complexes, for example by introducing a methyl or ethyl group on the phenyl substituents of the phosphorus atoms, could strongly improve their ionophoric activity.

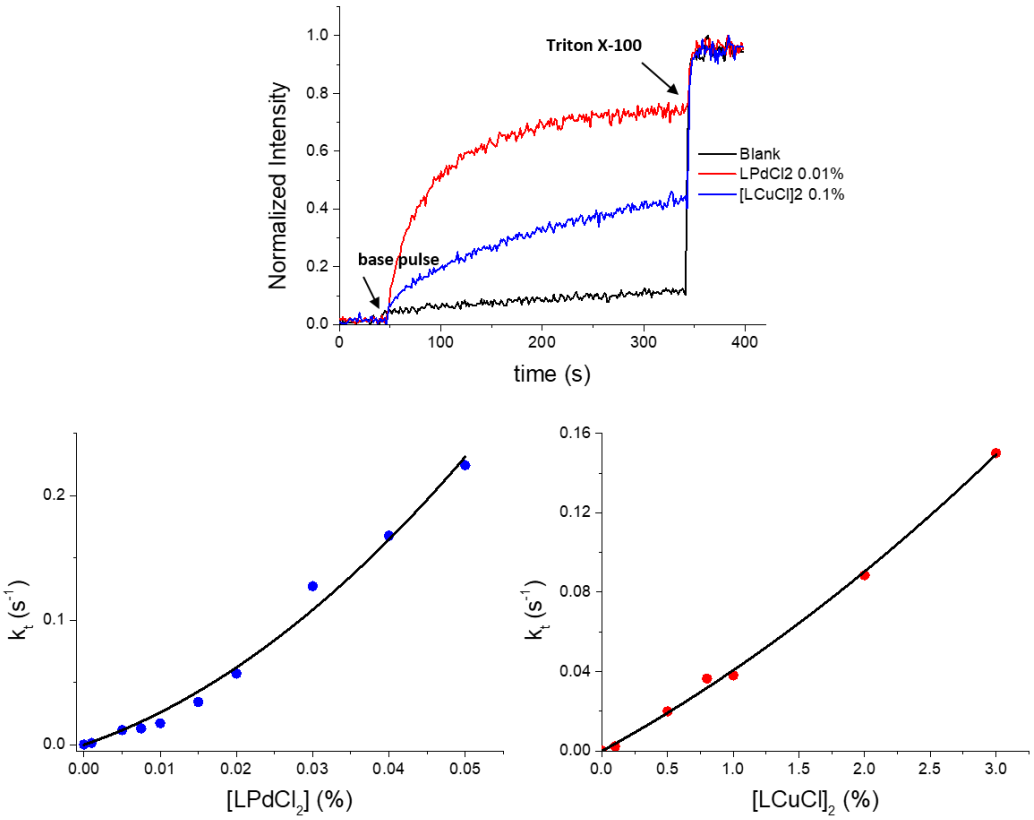

Figure 10. a) Normalized fluorescence change in HPTS fluorescence emission (FI) as a function of time after addition of the base (50 µL of 0.5 M NaOH) to EYPC LUVs (100 nm diameter) loaded with HPTS (0.1 mM HPTS, 0.17 mM total lipid concentration, 25 mM HEPES, 100 mM NaCl, pH 7.0, total volume 3 mL), in the presence of **[LPdCl$_2$]** (0.01% concentration, blue trace) and **[LCuCl]$_2$** (0.1% concentration, red trace). The concentration of the metal complexes is given in % with respect to the total concentration of lipids. b) and c) Dependence of the first order rate constant of the transport process (k_t, s^{-1}) on the concentration of **[LPdCl$_2$]** (b) and **[LCuCl]$_2$** (c). The original kinetics profiles are reported in Figure S12.

Conclusions

The sterically encumbered symmetrically substituted 4,5-bis(diphenylphosphino)acenaphthene ligand (**L**) is readily prepared in multigram scale from cheap organic precursors and through easy synthetic steps. Ligand **L** forms square planar complexes with group 10 metal ions (Ni(II), Pd(II), Pt(II)) and a dimeric tetrahedral complex with Cu(I). In all the complexes the rigid acenaphthene backbone forces the two phosphorus atoms at a distance well below than twice the van der Waals radius of P and a π-π interaction between two phenyl rings belonging to the two P atoms is present. The **[LCuCl]$_2$** complex exhibits weak fluorescence in solution with considerable solvatofluorochromism. In solid state, **[LCuCl]$_2$** displays higher photoluminescence quantum yield

due to the contribution of thermally-activated delayed fluorescence. At low temperature, this complex exhibits two phosphorescence emissions at 680 nm and 580 nm, arising from two distinct triplet states (CT and LCT respectively). **[LPdCl$_2$]** and **[LCuCl]$_2$** behave as chloride transporters across a liposomal phospholipid membrane with the Pd(II) complex displaying a high activity. This, together with the emission properties of the Cu(I) complex, make this scaffold a promising candidate for the development of highly active anion transporters. Work is in progress in this direction.

Experimental Section

The reagents and solvents have been purchased from Sigma-Aldrich or Alfa Aesar and used without further purification. Column chromatography was performed on silica gel 60 (Merck, 230–400 mesh ASTM), eluting with solvents mixtures as specified below. The reactions were monitored by TLC (silica gel/ UV 254, 0.20 mm, glass or aluminum support). All solvents used for spectroscopy measurements were of spectroscopic grade and used as acquired without further purification. UV-Vis spectra were recorded on an Agilent Cary 60 spectrometer or a Shimadzu UV-3600 double beam spectrophotometer in a quartz cuvette (1 cm optic path length). Fluorescence emission spectra and kinetics were recorded on a Varian Cary Eclypse or a Jobin Yvon Fluorolog spectrofluorimeter in a quartz cuvette (1 cm optic path length). Time-resolved emission spectra were collected in a Jobin Yvon Fluorolog fluorescence spectrometer with a pulsed Xenon lamp with full-width at half-maximum of 3 μs. Decays were collected with a minimum 100 μs delay to remove any interference from the lamp. For solid state spectroscopy, compound **[LCuCl]$_2$** was drop-cast from DCM onto a 1 × 3 cm quartz plate and the solvent was removed by slow evaporation under Argon. For measurements at 77K, the sample was placed in a model liquid nitrogen cryostat (Janis Research). Fluorescence decays of dyes were measured by the single-photon timing method using nanoLED (IBH) excitation at 343 nm, with 500 ps pulse width. The electronic start pulses are shaped in a constant fraction discriminator (Canberra 2126) and directed to a time to amplitude converter (TAC, Canberra2145). Emission wavelength was selected by a monochromator (Oriel 77,250) imaged in a fast photomultiplier (9814B Electron Tubes Inc.), the signal is shaped as before and delayed before entering the TAC as stop pulses. The analogue TAC signals were digitized. Data collections for X-ray structure determination were performed at the X-ray diffraction beamline (XRD1) of the Elettra Synchrotron, Trieste (Italy). Deposition Numbers 2012559 (**L**), 2012560 (**[LPtCl$_2$]**), 2012561 (**[LPdCl$_2$]**), 2012562 (**[LNiCl$_2$]**), 2012563 (**[LCuCl]$_2$**) contain the supplementary crystallographic data for this paper. These data are provided free of charge by the joint Cambridge Crystallographic

Data Centre and Fachinformationszentrum Karlsruhe Access Structures service (www.ccdc.cam.ac.uk/structures). Mass spectra have been acquired using a Bruker Esquire 4000 ESI-MS instrument or a Bruker micrOTOF-Q for HRMS by Dr. Fabio Hollan. Only molecular ions and major peaks are reported. Infrared spectra (IR) were measured on a Jasco FT/IR-200 instrument. NMR spectra were recorded on a Varian 500 MHz (125 MHz for carbon and 202 MHz for phosphorous) or a Varian 400 MHz (101 MHz for carbon and 162 MHz for phosphorous). Chemical shifts are reported as parts per million (ppm) relative to the solvent residual signal as internal reference. Coupling constants (J) are quoted in Hertz (Hz). The s, d, t, q, quint, sex, m, and bs signal notations indicate respectively: singlet, doublet, triplet, quartet, quintet, sextet, multiplet and broad signal. Elemental analyses were made by the Microanalysis Lab. at the University of Padova, Italy. by 5,6-Dibromo-acenaphtene was synthesized according to published literature.[36]

Synthesis of 5,6-bis(diphenylphosphino)acenaphthene (L)

5.00 g of 5,6-dibromoacenaphthene (MW=312.00 g/mol, 16.0 mmol, 1 eq.) were suspended in 50 mL of dry Et_2O under Ar atmosphere. The suspension was cooled at -78°C and 2.1 eq. of *n*BuLi (pentane solution 1.7M) were added slowly. The suspension was stirred at -78°C for 10 minutes and then it was brought at ambient temperature using a water bath. The reaction was monitored using TLC (EP) and, after the complete disappearing of the starting material, 7.17 mL of chlorodiphenylphosphine (MW=220.64 g/mol, d=1.23 g/mL, 40 mmol, 2.5 eq.) were added at -78°C. The solution was warmed up to ambient temperature and a copious amount of pale yellow precipitate formed. After 2 hours the precipitate was filtered through a glass sintered filter and washed with 10 mL of cold Et_2O. The precipitate was then dissolved with DCM and some LiCl was filtered off. The solvent was then removed under vacuum yielding 7.50 g of pure product as pale yellow solid (MW=522.57 gr/mol, 14.4 mmol, 90%).

^{1}H-NMR (400 MHz, $CDCl_3$): δ 7.28-7.23 (m, 24H), 3.43 (s, 4H); ^{1}H-NMR (400 MHz, CD_2Cl_2) δ: 7.30-7.21 (m, 16H), 7.20-7.15 (m, 8H), 3.41 (s, 4H); ^{13}C-NMR (101 MHz, CD_2Cl_2) δ: 149.2, 139.9, 139.8, 139.7, 138.6, 138.5, 138.2, 138.0, 133.8, 133.7, 133.6, 130.5, 130.4, 130.2, 128.3, 128.2, 128.1, 127.9, 119.9, 30.0; ^{31}P-NMR (162 MHz, $CDCl_3$) δ: -17.7; ^{31}P-NMR (162 MHz, CD_2Cl_2) δ: -16.2. IR: (KBr disc, cm^{-1}) ν = 3069m, 3049m, 2927m, 1603m, 1568m, 1478m, 1434s, 1326m, 1263w, 1186w, 1113w, 1089w, 1064w, 1028w, 844w, 744s, 699s. ESI-MS (m/z): 561.2 $[M+K]^+$.

Synthesis of [$LPdCl_2$]

5,6-Bis(diphenylphosphino)acenaphthene (200 mg, MW=522.57 g/mol, 0.383 mmol, 1.2 eq.) and 82 mg of $(MeCN)_2PdCl_2$ (MW=259.43 g/mol, 0.318 mmol, 1 eq.) were suspended in 10 mL of

MeOH. After a few minutes the suspension cleared up and it was stirred at ambient temperature for 3 hours. An abundant precipitate was formed. The precipitate was filtered and washed with Et_2O and dried under vacuum, yielding 135 mg (MW=699.89 g/mol, 0.193 mmol, 61%) of pure product.
^{1}H-NMR (400 MHz, $CDCl_3$) δ: 7.37 (m, 16H), 7.20 (m, 8H), 3.54 (s, 4H); ^{13}C-NMR (101 MHz, $CDCl_3$): 153.6, 140.1, 134.1, 134.0, 133.9, 130.9, 128.4, 128.3, 128.2, 120.6, 30.5; ^{31}P-NMR (162 MHz, $CDCl_3$) δ: 16.8. IR: (KBr disc, cm^{-1}) ν = 3075w, 3050m, 2922m, 1596m, 1480m, 1436s, 1338w, 1263w, 1099s, 1048w, 999w, 853w, 824w, 746m, 731m, 692s. ESI-MS (m/z): 665.0 $[M-Cl]^+$. Elemental Anal.: Calcd. for $C_{36}H_{28}Cl_2P_2Pd$: 61.78; H, 4.03; Found: C, 61.16; H, 3.94.

Synthesis of [$LPtCl_2$]

5,6-Bis(diphenylphosphino)acenaphthene (200 mg, MW=522.57 g/mol, 0.383 mmol, 1.2 eq.) and 120 mg of $Pt(cod)Cl_2$ (MW=374.16 g/mol, 0.318 mmol, 1 eq.) were suspended in 10 mL of MeOH. After a few minutes the suspension cleared up and it was stirred at ambient temperature for 3 hours. An abundant precipitate was formed. The precipitate was filtered and washed with Et_2O and dried under vacuum, yielding 175 mg (MW=788.55 g/mol, 0.223 mmol, 70%) of pure product.
^{1}H-NMR (400 MHz, CD_2Cl_2) δ: 7.36-7.166 (m, 20H), 3.48 (s, 4H); ^{13}C-NMR (101 MHz, $CDCl_3$): 152.9, 139.3, 134.0, 133.9, 133.8, 130.8, 128.1, 128.0, 127.9, 120.4, 120.3, 120.2, 30.4; ^{31}P-NMR (162 MHz, $CDCl_3$) δ: -2.0 (s), -2.0 (d, $J_{P\text{-}Pt}$ = 3327 Hz). IR: (KBr disc, cm^{-1}) ν = 3077w, 3052m, 2921m, 1600m, 1480m,1436s, 1338w, 1265w, 1097s, 1051w, 1000w, 851w, 826w, 745m, 732m, 693s. ESI-MS (m/z): 753.1 $[M-Cl]^+$. Elemental Anal.: Calcd. for $C_{36}H_{28}Cl_2P_2Pt$: C, 54.83; H, 3.58; Found: C, 54.90; H, 3.54.

Synthesis of [$LNiCl_2$]

5,6-Bis(diphenylphosphino)acenaphthene 200 mg (MW=522.57 g/mol, 0.383 mmol, 1.2 eq.) and 75 mg $NiCl_2 \cdot 6H_2O$ (MW=237.69 g/mol, 0.318 mmol, 1 eq.) were suspended in 10 mL of MeOH and stirred at ambient temperature for 3 hours. An abundant red precipitate was formed. The precipitate was filtered, washed with Et_2O, and dried under vacuum yielding 176 mg (MW=652.16 g/mol, 0.270 mmol, 85%) of pure product.
^{1}H-NMR (400 MHz, $CDCl_3$) δ: 7.71-6.93 (m, 20H), 3.90 (bs, 2H), 3.35 (bs, 2H); ^{13}C-NMR (101 MHz, $CDCl_3$): 154.2, 140.2, 137.8, 134.6, 134.2, 134.0, 132.7, 128.5, 128.4, 128.3, 127.6, 121.6, 120.7, 120.2, 30.1, 29.9, 29.8.; ^{31}P-NMR (162 MHz, $CDCl_3$) δ: -9.2. IR: (KBr disc, cm^{-1}) ν = 3056m, 2919m, 1600s, 1479m, 1436s, 1338w, 1264w, 1094m, 1049w, 1025w, 999w, 848m, 825w, 742s, 693s. ESI-MS (m/z): 615.1 $[M-Cl]^+$. Elemental Anal.: Calcd. for $C_{36}H_{28}Cl_2NiP_2$: C, 66.30; H, 4.33; Found: C, 66.15; H, 4.25.

Synthesis of $[LCuCl]_2$

105 mg of 5,6-bis(diphenylphosphino)acenaphthene (MW=522.57 g/mol, 0.200 mmol, 1 eq.) and 20 mg of CuCl (MW=98.999 g/mol, 0.20 mmol, 1 eq.) were suspended in 20 mL of $CHCl_3$. The mixture was stirred for 1 hour. The volume of the solvent was reduced to approximately 5 mL and then Et_2O was added in order to promote crystallization. The solution was kept in the fridge overnight, affording golden crystals. The suspension was filtered affording 68 mg (MW=1240.13 g/mol, 0.055 mmol, 55%) of pure product as golden powder. The ^{13}C-NMR was not recorded due to the low solubility of the compound. The peaks in the ^{1}H-NMR spectrum are very broad and it was not possible to correctly measure the peaks integral. Also the ^{31}P-NMR signal is broad.

^{1}H-NMR (400 MHz, CD_2Cl_2) δ: 7.40-6.95 (bs), 6.67 (bs), 3.45 (bs); ^{31}P-NMR (162 MHz, CD_2Cl_2) δ: -17.6 (bs). IR: (KBr disc, cm^{-1}) ν = 3045m, 2918m, 1611m, 1587m, 1480m, 1432s, 1377m, 1315m, 1265m, 1180m, 1095m, 1024mw, 999w, 846w, 818w, 740s, 692s, 665m. ESI-MS (m/z): 585.1 $[M\text{-}Cl]^+$, 1205.1 $[2M\text{-}Cl]^+$; Elemental Anal.: Calcd. For $C_{72}H_{56}Cl_2Cu_2P_4$: C, 69.56; H, 4.54; Found: C, 69.02; H, 4.51; ICP: Calculated: Cu, 10.22; P, 9.97; Measured: Cu, 10.28; P, 9.82

Ion transport studies

Egg yolk phosphatidylcholine (PC, 100 mg/mL chloroform solution) and 8-hydroxypyrene-1,3,6-trisulfonic acid trisodium salt (HPTS) were from Sigma; Triton® X-100 and HEPES buffer were from Fluka; all salts were of the best grade available from Aldrich and were used without further purification. Liposomes were prepared by extrusion using a 10 mL LipexTM Thermobarrel EXTRUDER (Northern Lipids Inc.) connected to a thermostatic bath kept at 25 °C. The 100 nm polycarbonate membranes were Nucleopore Track-Etch Membranes from Whatman. Fluorescence spectra were recorded on a Varian Cary Eclipse fluorescence spectrophotometer. All fluorimetric measurements were performed at 25 °C. The ionophores concentration is given in percent with respect to the total concentration of lipids. Mother solutions of ionophores were prepared in DMSO. Control experiments showed that the amount of DMSO added to the vesicular suspension in the different experiments (maximum amount 8% in volume) did not affect the permeability of the membrane.

150 µL of PC chloroform solution (100 mg/mL, 20 µmol) was first evaporated under Ar-flux to form a thin film and then dried under high vacuum for 3 h. The lipid cake was hydrated in 1.5 mL of 0.1 mM HPTS solution (HEPES 25 mM, 100 mM NaCl, pH 7) for 30 min at 40°C. The lipid suspension was submitted to 5 freeze-thaw cycles (-196°C/40°C) using liquid nitrogen and a thermostatic bath, and then extruded under nitrogen pressure (15 bar) at room temperature (10 extrusions through a 0.1 µm polycarbonate membrane). The LUV suspension was separated from

extravesicular dye by size exclusion chromatography (SEC) (stationary phase: pre-packed column Sephadex™ G-25, mobile phase: HEPES buffer 25 mM, 100 mM NaCl, pH 7) and diluted with HEPES buffer (HEPES 25 mM, 100 mM NaCl, pH 7) to give a stock solution with a lipid concentration of 5 mM (assuming 100% of lipids were incorporated into liposomes). 104 µL of the lipid suspension were placed in a fluorimetric cell and diluted to 3040 µL with HEPES buffer (HEPES 25 mM, 100 mM NaCl, pH 7). The total lipid concentration in the fluorimetric cell was 0.17 mM. An aliquot of solution of the ionophore in DMSO (10-80 µL of the appropriate mother solution in order to obtain the desired molcompound/mollipid ratio) was then added to the lipid suspension and the cell was incubated at 25°C for 10 min. After incubation, the time course of fluorescence was recorded for 50 s monitoring the HPTS emission at 510 nm with excitation wavelengths set alternatively at 403 and 460 nm on a 0.5+0.5 s cycle. Then 50 µL of 0.5 M NaOH were rapidly added through an injector port and the fluorescence emission was recorded for 350 s. In each experiment, maximal changes in dye emission were obtained by final lysis of the liposomes with a detergent (40 µL of 5% aqueous Triton® X-100). The data set consists of emission intensities at 510 nm modulated by alternating excitation at 403 nm and 460 nm on a 0.5+0.5 s cycle. The concentration of the conjugate base form of HPTS is related to the emission intensity at 510 nm during the period in which the dye is excited at 460 nm (E_{460}) while the concentration of the protonated form is related to the emission intensity at 510 nm during the period in which the dye is excited at 403 nm (E_{403}). Fluorescence time courses were normalized using the following equation, where the subscripts 0, ∞ and t denote the emission ratio before the base pulse, after detergent lysis, and at an intermediate time, respectively.

$$FI = \frac{\left(\frac{E_{403}}{E_{460}}\right)_t - \left(\frac{E_{403}}{E_{460}}\right)_0}{\left(\frac{E_{403}}{E_{460}}\right)_\infty - \left(\frac{E_{403}}{E_{460}}\right)_0} \times 100$$

Acknowledgments

PT thanks Prof. Enzo Alessio, Prof. Barbara Milani and Dr. Alessio Vidal of the University of Trieste for fruitful discussion. MT, AJP and PT thank the EU for the MC-RISE INFUSION research project (grant N. 734834). This work was supported by the Associate Laboratory for Green Chemistry - LAQV which is financed by portuguese FCT/MCTES (UIDB/50006/2020). FCT is also acknowledged for supporting the National Portuguese NMR Network (RECI/BBB-BQB/0230/2012), and for funding under grant SFRH/BPD/120599/2016 (JA) and project PTDC/QUI-QFI/32007/2017 (JA).

Keywords: Phosphane ligands, Acenaphthene, Metal complexes, Ionophores, TADF

References

[1] K. Issleib, D.-W. Müller, *Chem. Ber.* **1959**, *92*, 3175−3182.

[2] M. N. Birkholz, Z. Freixa, P. van Leeuwen, *Chem. Soc. Rev.* **2009**, *38*, 1099−1118.

[3] Z. Freixa, P. van Leeuwen, *Coord. Chem. Rev.* **2008**, *252*, 1755−1786.

[4] M. Dutartre, J. Bayardon, S. Juge´, *Chem. Soc. Rev.* **2016**, *45*, 5771−5794.

[5] S. Luhr, J. Holz, A. Borner, *ChemCatChem* **2011**, *3*, 1708−1730.

[6] R. Noyori, *Angew. Chem, Int. Ed.* **2013**, *52*, 77−92.

[7] S. L. James, *Chem. Soc. Rev.* **2009**, *38*, 1744−1758.

[8] R. Chakrabarty, P.S. Mukherjee, P.J. Stang, *Chem. Rev.* **2011**, *111*, 6810−6918.

[9] E. Iengo, P. Cavigli, D. Milano, P. Tecilla, *Inorg. Chim. Acta* **2014**, *417*, 59−78.

[10] F. De Riccardis, I. Izzo, D. Montesarchio, P. Tecilla, *Acc. Chem. Res.* **2013**, *46*, 2781–2790.

[11] M. Boccalon, E. Iengo, Paolo Tecilla, *J. Am. Chem. Soc.* **2012**, *134*, 20310−20313.

[12] D. Milano, L. Đorđević, E. Zangrando, E. Iengo, P. Tecilla, *Inorg. Chim. Acta* **2016**, *453*, 376–384.

[13] D. Milano, B. Benedetti, M. Boccalon, A. Brugnara, E. Iengo, P. Tecilla, *Chem. Commun*. **2014**, *50*, 9157−9160.

[14] M. Tosolini, "Transition Metal Complexes as Anion Carriers" (2018). Electronic Thesis and Dissertation Repository. http://hdl.handle.net/11368/2939507

[15] B. A. Chalmers, K. S. Athukorala Arachchige, J. K. D. Prentis, F. R. Knight, P. Kilian, A. M. Z. Slawin, J. D. Woollins, *Inorg. Chem.* **2014**, *53*, 8795−8808.

[16] P. Kilian, F. R. Knight, J. D. Woollins, *Chem. Eur. J.* **2011**, *17*, 2302 – 2328.

[17] P. Kilian, F. R. Knight, J. D. Woollins, *Coord. Chem. Rev.* **2011**, *255*, 1387−1413.

[18] F. R. Bregman, J. M. Ernsting, F. Müller, M. D. K. Boele, L. A. van der Veen, C. J. Elsevier, *J. Organomet. Chem.* **1999**, *592*, 306−311.

[19] K. S. Athukorala Arachchige, P. Sanz Camacho, M. J. Ray, B. A. Chalmers, F. R. Knight, S. E. Ashbrook, M. Bühl, P. Kilian, A. M. Z. Slawin, J. D. Woollins, *Organometallics* **2014**, *33*, 2424−2433.

[20] B. A. Chalmers, C. B. E. Meigh, P. S. Nejman, M. Bühl, T. Lébl, J. D. Woollins, A. M. Z. Slawin, P. Kilian, *Inorg. Chem.* **2016**, *55*, 7117−7125.

[21] M. J. Ray, M. Bühl, L. J. Taylor, K. S. Athukorala Arachchige, A. M. Z. Slawin, P. Kilian, *Inorg. Chem. 2014*, **53**, 8538−8547.

[22] L. J. Taylor, M. Bühl, P. Wawrzyniak, B. A. Chalmers, J. D. Woollins, A. M. Z. Slawin, A. L. Fuller, P. Kilian, *Eur. J. Inorg. Chem.* **2016**, 659−666.

[23] L. J. Taylor, M. Bühl, B. A. Chalmers, M. J. Ray, P. Wawrzyniak, J. C. Walton, D. B. Cordes, A. M. Z. Slawin, J. D. Woollins, P. Kilian, *J. Am. Chem. Soc.* **2017**, *139*, 18545−18551.

[24] E. Hupf, E, Lork, S. Mebs, L. Chęcińska, J. Beckmann, *Organometallics* **2014**, *33*, 7247−7259.

[25] B. A. Chalmers, P. S. Nejman, A. V. Llewellyn, A. M. Felaar, B. L. Griffiths, E. I. Portman, E.-J. L. Gordon, K. J. H. Fan, J. D. Woollins, M. Bühl, O. L. Malkina, D. B. Cordes, A. M. Z. Slawin, P. Kilian, *Inorg. Chem.* **2018**, *57*, 3387−3398.

[26] Effendy, C. Di Nicola, M. Fianchini, C. Pettinari, B. W. Skelton, N. Somers, A. H. White, *Inorg. Chim. Acta* **2005**, *358*, 763−795.

[27] M. Mantina, A. C. Chamberlin, R. Valero, C. J. Cramer, D. G. Truhlar, *J. Phys. Chem. A* **2009**, *113*, 5806−5812.

[28] R. D. Jackson, S. James, A. G. Orpen, P. G. Pringle, *J. Organomet. Chem.* **1993**, *458*, C3.

[29] W. Śmiszek-Lindert, A. Michta, A. Tyl, G. Małecki, E. Chełmecka, S. Maślanka, *J. Serb. Chem. Soc.* **2015**, 80, 1489−1504.
[30] S. E. Wheeler, *J. Am. Chem. Soc.* **2011**, *133*, 10262–10274.
[31] G. Accorsi, N. Armaroli, B. Delavaux-Nicot, A. Kaeser, M. Holler, J.-F. Nierengarten, A. Degli Esposti, *J. Mol. Stru. THEOCHEM* **2010**, *962*, 7–14.
[32] R. Czerwieniec, H. Yersin, *Inorg. Chem.* **2015**, 54, 4322–4327.
[33] F. B. Dias, K. N. Bourdakos, V. Jankus, K. C. Moss, K. T. Kamtekar, V. Bhalla, J. Santos, M. R. Bryce, A.P. Monkman, *Adv. Mater.* **2013**, *25*, 3707–3714.
[34] M. Tosolini, P. Pengo, P. Tecilla, *Curr. Med. Chem.* **2018**, *25*, 3560–3576.
[35] N. Sakai, S. Matile, *J. Phys. Org. Chem.* **2006**, *19*, 452–460.
[36] T. Norio, K. Toshiyasu, *Bull. Chem. Soc. Jpn.* **1981**, *54*, 3020–3025.

Key Topic: Diphosphine ligands

Table of Contents

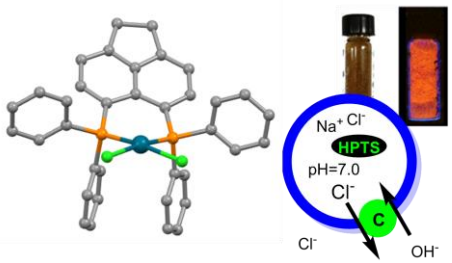

The sterically encumbered symmetrically substituted 4,5-bis(diphenylphosphino)acenaphthene ligand forms distorted square planar complexes with group 10 metal ions (Ni(II), Pd(II), Pt(II)) and a dimeric tetrahedral complex with Cu(I). The Cu(I) complex is weakly fluorescent and in the solid state exhibits thermally-activated delayed fluorescence and phosphorescence. Moreover, the Pd(II) and Cu(I) complexes behave as chloride carrier across a liposomal phospholipid membrane.